Development of a flame propagation model for dual-fuel partially premixed compression ignition engines

S Singh*, **L Liang, S-C Kong,** and **R D Reitz**
Engine Research Center, The University of Wisconsin, Madison, Wisconsin, USA

The manuscript was accepted after revision for publication on 10 February 2005.

DOI: 10.1243/146808705X7464

Abstract: The limitations of an existing characteristic–time combustion (CTC) model are explored and a new combustion model is developed and applied to simulate combustion in dual-fuel engines in which the premixed natural gas is ignited by the combustion flame initiated by a diesel spray. The model consists of a diesel auto-ignition model and a flame propagation model. A *G*-equation-based model previously developed to simulate SI engine combustion was incorporated with an auto-ignition model to simulate the flame propagation process in partially premixed environments. The computer code is based on the KIVA-3V code and consists of updated sub-models to simulate more accurately the fuel spray atomization, auto-ignition, combustion, and emissions processes. Modifications were made to implement the level set *G*-equation approach and to track the location of the flame as a function of the turbulent flame speed, flame curvature, flow velocity, and the movement of the computational mesh in the engine environment. Good agreement with engine experiments was obtained by using the present model.

Keywords: flame propagation, dual-fuel engines, emissions, *G*-equation

1 INTRODUCTION

Natural gas is regarded as a viable alternative to liquid petroleum fuels. Compression ignition engines running on natural gas as the primary fuel produce low oxides of nitrogen (NO_x) and particulate emissions [**1**, **2**]. Use of compressed natural gas in compression ignition engines does not require extensive modifications to the system. Diesel engines may be readily converted to operate primarily on natural gas using diesel pilot injection to achieve ignition. However, careful design is required to prevent excessive diesel fuel usage and high hydrocarbon (HC) emissions. A well-configured pilot-ignited dual-fuel engine shows significant potential to rival diesel engines in their thermal efficiency and exhaust emissions.

Experimental research in dual-fuel engines has concentrated on defining the extent of dual fuelling and its effects on emissions and performance [**2**, **3**]. It is found that increased natural gas energy substitution is very effective in NO_x reduction [**4**] but engine operation can suffer from high HC emissions and poor performance, especially at light loads [**5**, **6**].

In addition to experiments, there have been efforts to develop computer models to help understand the dual-fuel combustion process. Models as simple as phenomenological and as detailed as computational fluid dynamics (CFD) models have been proposed by various researchers. For example, a two-zone model was developed to simulate diesel/natural gas combustion using a semi-empirical spray model for diesel spray simulation by Hountalas and Papagiannakis [**7**]. Natural gas injection, mixing, and spark ignition parameters were also studied using a one-step global reaction for combustion simulation [**8**]. A multi-dimensional CFD model with a mixing-controlled timescale combustion model has also been developed to study the diesel spray and natural gas combustion processes of a dual-fuel engine [**1**, **9**].

Methane is the simplest but not a typical HC fuel. A tremendous amount of attention has been paid to studying its chemical kinetic mechanism. There have been fundamental studies on natural gas ignition

* *Corresponding author: Engine Research Center, Department of Mechanical Engineering, The University of Wisconsin, Madison, WI53726, USA. email: singh002@erc.wisc.edu*

and combustion chemistry in recent years. The auto-ignition of methane was studied experimentally to obtain ignition delay data as a function of engine cylinder pressure and temperature by the Sandia group [**10**, **11**]. Detailed chemical kinetic mechanisms for methane oxidation have also been developed [**12–14**]. But computational time and storage constraints place severe restrictions on the complexity of the chemical kinetic mechanism that can be used for detailed chemistry calculations. Reaction mechanisms involving a small number of species and reactions are used to cut the calculation time while maintaining the overall accuracy of the predictions. A one-step global reaction representing the overall combustion through species fuel, CO, CO_2, H_2, and H_2O is also used [**15**].

The objective of the present research was to develop a model to simulate diesel/natural gas combustion in dual-fuel engines. Realizing the possibility of flame propagation in premixed mixtures, a flame propagation model based on the level set method of Peters [**16**] and Tan and Reitz [**17**] was implemented into the KIVA-3V diesel engine CFD code. The new model was validated by comparing with the experimental engine data.

2 EXPERIMENTAL SET-UP

The engine used in the present study was a Caterpillar single cylinder, four-stroke, direct injection diesel engine with the specifications given in Table 1 [**1**, **6**]. A schematic diagram of the engine set-up is shown in Fig. 1. The engine was coupled to a d.c. dynamometer and the experiments were carried out at a constant speed of 1700 r/min. Turbocharged engine operation was simulated by controlling the intake air and exhaust pressures. The intake temperature and pressure were chosen to give stable but knock-free engine operation based on previous studies [**4**]. A common-rail injection system was used for diesel injection with a nozzle hole size of 0.15 mm. Crank-angle-resolved in-cylinder pressure and the diesel injection pressure were measured. The primary engine fuel, i.e. natural gas, was a mixture of 98.3 per cent methane, 1.3 per cent nitrogen, and less than 1 per cent ethane and carbon dioxide. The natural gas was injected into the intake manifold and its flowrate was controlled by a thermal mass flow controller. The air flowrate was measured using a laminar flow element. The power output of the engine was maintained constant by controlling the natural gas mass flowrate. Engine exhaust NO_x and HC emissions were also measured. Details of the experimental set-up and the emissions measurement system are given by Singh *et al.* [**1**].

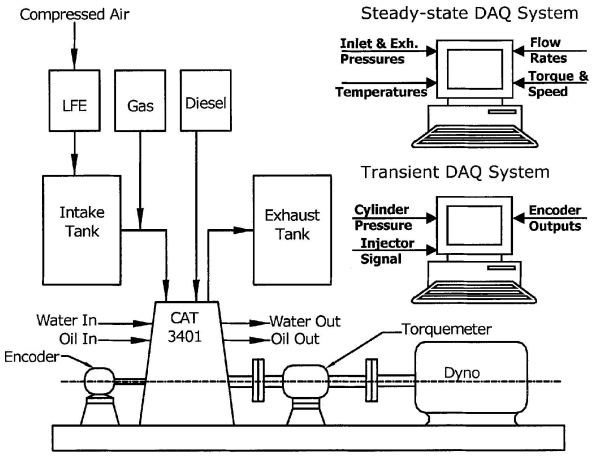

Fig. 1 Experimental set-up

3 COMPUTATIONAL GEOMETRY

The piston geometry and computational mesh used for the simulations are shown in Fig. 2. A 90° sector mesh with cell density of 24 000 cells was used in

Table 1 Engine specifications

Parameter	Specification
Engine type	Single-cylinder, four-cycle, simulated turbo-charging
Bore × stroke (cm)	13.7 × 16.5
Displacement, L	2.43
Compression ratio	14.5 : 1
Primary fuel	Compressed natural gas
Gas supply	Intake port, 207 kPa
Ignition source	Diesel pilot
Fuel injection	Diesel injection
Injection system	After-market electronically controlled common-rail
Number of nozzles	4
Combustion chamber	Bowl in piston
Number of valves per cylinder	4
Rated power (kW)	42@2100 r/min

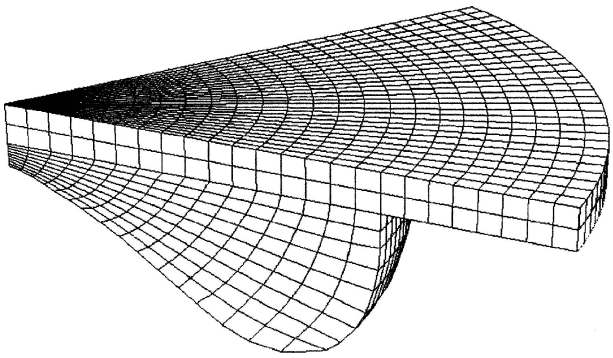

Fig. 2 Computational mesh

this study, considering that the diesel injector has four nozzle holes. The mesh was created using a standard KIVA-3V pre-processor. This mesh resolution has been found to give adequately grid-independent results [**17–20**]. The diesel fuel injection rate shape acquired from the experiments was used for simulating diesel pilot injection. The falling-type injection rate profile shown in Fig. 3 provides the maximum injection velocities at the start of injection and the minimum at the end of injection. The computations were started from intake valve closure (IVC) assuming a uniform mixture distribution. Therefore, in the case of dual-fuel combustion, a homogeneous natural gas and air mixture was assumed to exist in the cylinder at the start of the simulations.

4 MOTIVATION

In previous work, the authors presented results of applying a mixing-controlled turbulent timescale diesel combustion model to dual-fuel combustion [**1**, **9**]. This conventional diesel combustion model performed reasonably well under high diesel pilot conditions ($\geqslant$10 per cent diesel) in which the lean premixed natural gas was burned as a result of high in-cylinder temperatures and turbulent flows created by the significant diesel spray injection. However, as the amount of diesel fuel was reduced to a very small quantity, for example 3 per cent by energy, as is of particular interest in applications, the energy released by the natural gas mixture was not well predicted, as shown in Fig. 4 [**1**]. Figure 4 shows experimental and predicted in-cylinder pressure for 10 per cent and 3 per cent diesel pilot quantities. It can be observed that the pressure trace is reasonably well reproduced for the higher diesel pilot quantity case when compared with the case with very small diesel pilot quantity. To understand the limitation of the characteristic–time combustion (CTC) model in predicting combustion under conditions of very low pilot quantity, one needs to visualize in-cylinder combustion and relate it to the CTC model formulation. Figure 5 shows in-cylinder temperature contours

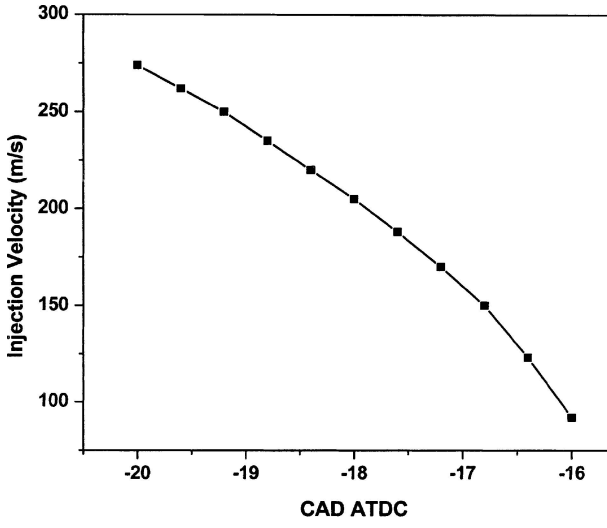

Fig. 3 Injection profile

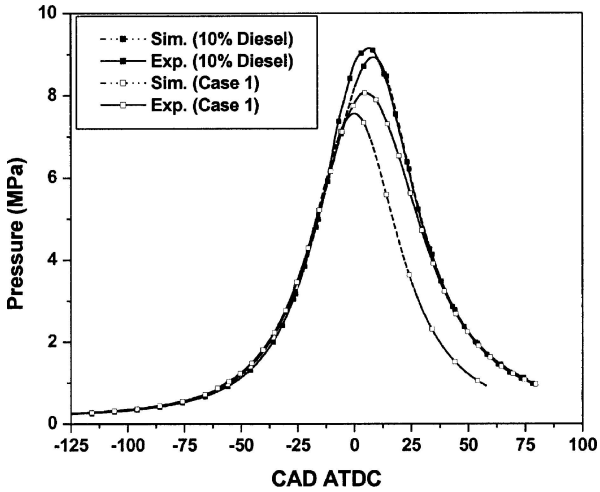

Fig. 4 Cylinder pressure for 10 per cent and 3 per cent diesel pilot quantities using the conventional diesel combustion model

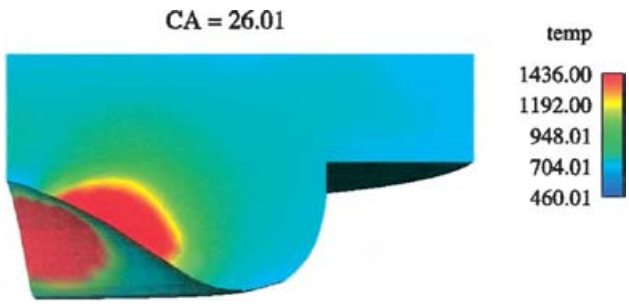

Fig. 5 Cylinder gas temperature for 3 per cent diesel pilot quantity using the conventional diesel combustion model

for the 3 per cent diesel pilot quantity obtained by using the CTC combustion model. It can be observed that the high-temperature zone produced by the diesel fuel combustion is confined to a very small location near the floor of the piston bowl in the combustion chamber. This high-temperature zone is the result of combustion of diesel fuel and natural gas in its vicinity. Diesel is assumed to ignite first due to its low ignition temperature. Natural gas is consumed locally due to the high temperature resulting from diesel ignition. At small diesel pilot conditions, a premixed natural gas mixture is most likely burned as a result of a flame propagation process that is not well simulated by the timescale diesel combustion model. In this case, a flame propagation model is needed to simulate the dual-fuel combustion process. Unlike in the case of spark ignition engines where a flame is initiated at a fixed location by a spark plug, in the present case the flame is initiated by auto-ignition of diesel pilot injection at unspecified locations in the combustion chamber. If the ignition source is robust enough that the energy released from ignition can compete with the heat loss to the surroundings, the ignition source can develop into a propagating flame. It is also possible for multiple flames to appear simultaneously at different locations in the combustion chamber. These considerations add complexity to the model formulation.

5 MODEL FORMULATION

The CFD model used in this study is based on the KIVA-3V code (Amsden [**21**]) with improvements in various sub-models, including improved spray atomization, ignition, combustion (flame propagation), emissions, and wall heat transfer models [**18–20**, **22**]. Only the auto-ignition, combustion, and NO_x emissions models will be briefly described here. Emphasis will be given on the approach used to combine the auto-ignition model with a flame propagation model.

5.1 Ignition model

For simplicity, the Shell auto-ignition model [**23**] and a laminar and turbulent characteristic–time diesel combustion model [**22**] were used together to simulate the ignition process of diesel fuel prior to flame propagation. Detailed chemistry mechanisms could have been used, but the simpler model was deemed to be adequate for the present study.

5.1.1 Shell model

The Shell HC fuel auto-ignition model [**18**, **23**] was used to simulate the diesel ignition process. The model uses a simplified reaction mechanism consisting of eight generic reactions and five generic species. The reactions represent four types of elementary reaction steps that occur during the ignition process, namely, initiation, propagation, branching, and termination. The five generic species represent fuel, oxygen, radicals, intermediate species, and branching agents. The reactions account for the degenerate branching characteristics of HC fuels. The premise is that degenerative branching controls the two-stage ignition and cool flame phenomena seen during HC auto-ignition. A chain propagation cycle is formulated to describe the history of the branching agent together with one initiation and two termination reactions. Details of the model can be found in Kong and Reitz [**18**] and Kong *et al.* [**22**].

5.1.2 Characteristic–time combustion model

The CTC model was used in conjunction with the Shell model for predicting the ignition flame kernel development. The CTC model calculates the equilibrium concentration of each species and the corresponding laminar and turbulent characteristic times to determine species conversion rates [**22**]. Seven major combustion species are considered; fuel, O_2, N_2, CO_2, H_2O, and CO. The rate of change of the concentration of species i is given as

$$\frac{\mathrm{d}Y_\mathrm{i}}{\mathrm{d}t} = -\frac{Y_\mathrm{i} - Y_\mathrm{i}^*}{\tau_\mathrm{c}} \tag{1}$$

where Y_i is the concentration of species i, Y_i^* is the local and instantaneous thermodynamic equilibrium concentration, and τ_c is the chemical conversion time to achieve equilibrium. The chemical conversion time is calculated as the sum of a kinetic laminar timescale, τ_l, and a turbulent mixing timescale, τ_t, as follows:

$$\tau_\mathrm{c} = \tau_\mathrm{l} + f\tau_\mathrm{t} \tag{2}$$

The laminar timescale is derived from a one-step kinetic reaction rate, and is modelled as [**13**]

$$\tau_\mathrm{l} = \mathrm{A}^{-1}[\mathrm{C}_n\mathrm{H}_{2n+2}]^{0.75}[\mathrm{O}_2]^{-1.5}\exp\left(\frac{E}{R_\mathrm{u}T}\right) \tag{3}$$

where A is a constant equal to 1.5×10^5, E is the activation energy 18 479 cal/mol, R_u is the universal gas constant, and T is the local gas temperature. f is a progress variable ($0 \leqslant f \leqslant 1$) which simulates the influence of turbulence on combustion. $f = 0$ prior to combustion and $f = 1$ when combustion is completed. In the ignition model, only diesel fuel was

considered as the 'fuel'. During the ignition process, the value of f would be very small such that ignition is controlled by the chemical kinetics of the fuel only.

5.2 Combustion model

The premixed natural gas and air mixture is consumed by one or more turbulent flames that are initiated by the ignition of the diesel fuel. The main heat release occurs in a thin reaction sheet, i.e. a flame which separates the burned and unburned gases.

The flame front is tracked by a level set method that was developed primarily for premixed combustion [**16**, **17**]. The flame is a three-dimensional surface which is defined by $G(\vec{x}, t) = 0$. The scalar G divides the field into an unburned region ($G < 0$) and a burned region ($G > 0$). The form of G equation used here is given as

$$\frac{\partial \tilde{G}}{\partial t} + (\tilde{\boldsymbol{v}}_{\mathrm{bf}} - \boldsymbol{v}_{\mathrm{vertex}}) \cdot \nabla \tilde{G} = \frac{\bar{\rho}_{\mathrm{u}}}{\bar{\rho}} s_{\mathrm{t}}^{0} |\nabla \tilde{G}| - D_{\mathrm{t}} \tilde{k}_{\mathrm{M}} |\nabla \tilde{G}| \quad (4)$$

where $\tilde{\boldsymbol{v}}_{\mathrm{bf}}$ and $\boldsymbol{v}_{\mathrm{vertex}}$ are the fluid and mesh vertex velocities (with the moving mesh), D_{t} is the turbulent diffusivity, and $\tilde{k}_{\mathrm{M}}$ is the mean flame curvature [**24**] given as

$$\tilde{k}_{\mathrm{M}} = \nabla \cdot \left(- \frac{\nabla \tilde{G}}{|\nabla \tilde{G}|} \right) = - \frac{\begin{array}{r}[(\tilde{G}_{yy} + \tilde{G}_{zz})\tilde{G}_x^2 + (\tilde{G}_{xx} + \tilde{G}_{zz})\tilde{G}_y^2 + (\tilde{G}_{xx} + \tilde{G}_{yy})\tilde{G}_z^2 \\ - 2\tilde{G}_x \tilde{G}_y \tilde{G}_{xy} - 2\tilde{G}_x \tilde{G}_z \tilde{G}_{xz} - 2\tilde{G}_y \tilde{G}_z \tilde{G}_{yz}]\end{array}}{(\tilde{G}_x^2 + \tilde{G}_y^2 + \tilde{G}_z^2)^{3/2}} \quad (5)$$

The turbulent flame speed s_{t}^{0} is a function of the laminar flame speed s_{l}^{0} and the local flow conditions and was expressed as [**16**]

$$s_{\mathrm{t}}^{0} = s_{\mathrm{l}}^{0} + v' \left\{ - \frac{\mathrm{a_4 b_3^2}}{2\mathrm{b_1}} Da + \left[\left(\frac{\mathrm{a_4 b_3^2}}{2\mathrm{b_1}} Da \right)^2 + \mathrm{a_4 b_3^2} Da \right]^{1/2} \right\} \quad (6)$$

where v' is the turbulence intensity; $\mathrm{a_4} = 0.78$, $\mathrm{b_1} = 2.0$, and $\mathrm{b_3} = 1.0$ are constants derived from the turbulence model; and the DamKohler number Da is

$$Da = \frac{s_{\mathrm{l}}^{0} l}{v' l_{\mathrm{F}}} \quad (7)$$

l is the turbulence integral length scale obtained from the renormalization group (RNG) $\kappa - \varepsilon$ turbulence model, and

$$l_{\mathrm{F}} = \frac{(\lambda / c_{\mathrm{p}})_0}{(\rho s_{\mathrm{l}}^{0})_{\mathrm{u}}} \quad (8)$$

is the flame thickness. The heat conductivity λ and heat capacity c_{p} are evaluated at the inner layer temperature [**16**].

The flame speed was found to be very important in the predictions. Standard literature flame speed correlations did not provide satisfactory results in the present engine simulations. Figure 6 shows the laminar flame speed calculated from correlations given by Rahim *et al.* [**25**] at a fixed pressure of 8 MPa. The correlation predicts the lean and rich flammability limits of a methane–air mixture to be 0.45 and 1.6 respectively. Increased mixture temperature does not extend the flammability limit. For the experimental engine operating conditions, the equivalence ratio of a premixed methane–air mixture was as low as 0.35 (below the range of validity of the correlation). But the engine operation was found to be very stable and repeatable for these low equivalence ratios. This suggests that the mixture conditions inside the cylinder supported the propagation of a flame. Also, the computational results show that unburned charge temperatures as high as 1300–1400 K were seen ahead of the flame front. Therefore, it was concluded that available laminar flame speed correlations such as those of Rahim *et al.* [**25**] could not be used for this research. Thus, a laminar flame speed library was generated for natural gas using

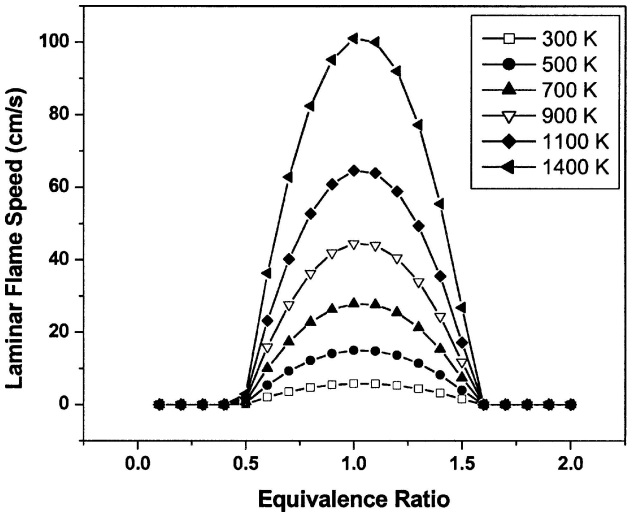

Fig. 6 Laminar flame speed for mixture of methane and air at 8 MPa as a function of equivalence ratio and unburned gas temperature calculated from correlation given by Rahim *et al.* [**25**]

the PREMIX code [**26**]. Figure 7 shows the predicted laminar flame speed as a function of unburned gas temperature T_u for different equivalence ratios at a representative pressure of 8 MPa. The data library included pressures up to 10 MPa. It can be observed that under high-temperature conditions the lean and rich flammability limits are extended widely.

The species density change in the computational cell containing the mean flame front was given as [**24**]

$$\frac{dY_i}{dt} = (Y_i^u - Y_i^b)\frac{A}{V}s_t^0 \tag{9}$$

where A is the flame surface area and V is the cell volume. Y_i is the species mass fraction and the superscripts u and b refer to their values in the $G<0$ and $G>0$ regions respectively. The rate of conversion behind the flame is calculated by equation (1) using the turbulent timescale only [**24**].

To extend the original diesel combustion model to dual-fuel combustion, a new species i.e. methane was added to the species array. The amount of diesel fuel and methane were lumped together as 'fuel' before applying reaction equations. After the application of equations (1) and (9), the remaining 'fuel' was redistributed back to both diesel fuel and methane according to their original proportions. In such a formulation, it is inherently assumed that the conversion rates of diesel fuel and methane are the same, which is a reasonable assumption.

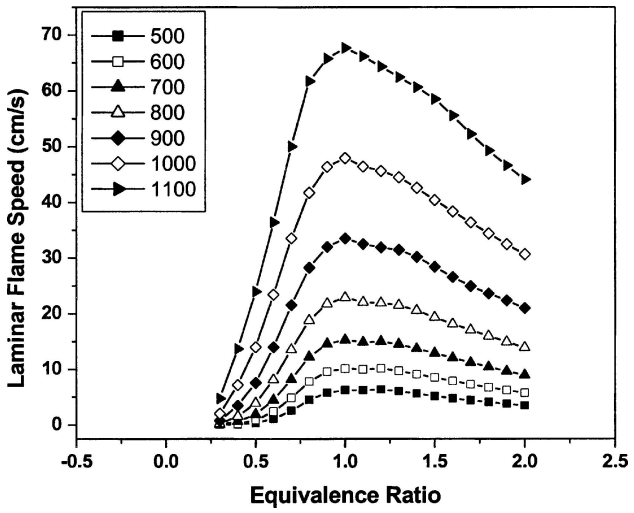

Fig. 7 Laminar flame speed for mixture of methane and air at 8 MPa as a function of equivalence ratio and unburned gas temperature calculated by the PREMIX code

5.3 NO_x model

The formation of NO_x emissions was predicted by using the extended Zel'dovich mechanism that accounts for only thermal NO_x in the post-flame regions. The three reactions of the extended Zel'dovich mechanism are [**27**]

$$\begin{aligned} &O + N_2 \underset{k_1^-}{\overset{k_1^+}{\rightleftarrows}} NO + N \\ &N + O_2 \underset{k_2^-}{\overset{k_2^+}{\rightleftarrows}} NO + O \\ &N + OH \underset{k_3^-}{\overset{k_3^+}{\rightleftarrows}} NO + H \end{aligned} \tag{10}$$

Assuming steady state concentration for atomic nitrogen (N), the rate of NO formation can be written as [**27**]

$$\frac{d[NO]}{dt} = 2k_1^+[O][N_2]\frac{1-[NO]^2/(K)[O_2][N_2]}{1+k_1^-[NO]/(k_2^+[O_2]+k_3^+[OH])} \tag{11}$$

where

$$k = \left(\frac{k_1^+}{k_1^-}\right)\left(\frac{k_2^+}{k_2^-}\right)$$

In the model, minor species O and OH were assumed to be in equilibrium.

6 SOLUTION ALGORITHM

1. The Shell and CTC models were used to predict the ignition of diesel fuel and the formation of the ignition kernel. These models were used only in unburned regions, i.e. $G<0$. The Shell model was used at low temperatures ($T<1000$ K) and the CTC model was used at high temperatures ($T>1000$ K) until a fully developed flame was formed. The ignition process was thus initially controlled by chemical kinetics and turbulence had no effect until the later stage, as dictated by the progress variable f in equation (1).
2. As soon as an ignition kernel was formed, the combustion model was activated by initialization of the scalar G. The criterion used was that computational cells with temperatures greater than 1200 K were regarded as ignition sites. This temperature was chosen to account for the 300–400 K rise in temperature because of ignition. In these cells, an ignition kernel radius was found from the volume of the adjacent high-temperature cells and when the ignition kernel radius R was larger than the in-cylinder average turbulent integral

length scale, a $G(\boldsymbol{x}, t) = 0$ surface was initialized. Within the $G(\boldsymbol{x}, t) = 0$ surface, the gas temperature is thus higher than 1200 K and outside the surface it is lower than 1200 K (Fig. 8). The value of G at each vertex is assigned as a signed distance function

$$\tilde{G}(\tilde{\boldsymbol{x}}, t) = \pm\sqrt{(x(k)-x_{\mathrm{p}}(k))^2+(y(k)-y_{\mathrm{p}}(k))+(z(k)-z_{\mathrm{p}}(k))} \quad (12)$$

G is positive when the vertex is inside the flame kernel and negative when the vertex is outside. x_{p}, y_{p}, and z_{p} are x, y, and z coordinates of any location k on the $G(\boldsymbol{x}, t) = 0$ surface.

3. After a $G(\boldsymbol{x}, t) = 0$ surface was initiated, equation (4) was solved to locate the flame front. In the level set method, only $G(\boldsymbol{x}, t) = 0$ (i.e. the flame front location) has physical meaning. The condition $|\nabla G| = 1$ was applied to renormalize the level set for $G(\boldsymbol{x}, t) \neq 0$ at each time step [**17**].

7 RESULTS AND DISCUSSION

The computations started from intake valve closure (IVC) assuming a uniform mixture distribution, and a homogeneous natural gas and air mixture was specified at the start of the simulations. Representative power loadings of the engine, i.e. half and full loads, were used for the model validation. In the experiments the intake temperature and pressure were chosen to give stable but knock-free engine operation based on previous research [**4**] and the test conditions are listed in Table 2. The quantity of diesel pilot fuel is less than or equal to 3 per cent of the total fuel by energy content.

Figure 9 shows the results of cylinder pressure and heat release rate for case 1, i.e. start of diesel injection at -20° ATDC. Diesel fuel ignites at about -5° ATDC and accounts for the early part of the heat release, as predicted by the ignition model. The simulations predict that the combustion model is activated at about -3° ATDC and after ignition the heat release occurs mainly at the flame front and around the reaction zone, as simulated by the G-equation combustion model. Figure 10 shows the structure of the turbulent flame at the time of ignition and at a later stage near the end of the combustion (35° ATDC). A maximum turbulent flame speed of about 5 m/s was observed. The tail of the heat release curve seen in Fig. 9 indicates slow but steady combustion at the late stages of combustion as a result of the decreasing gas temperature and the fact that the flame reaches the walls. Due to the low equivalence ratio in the premixed natural gas/air mixture, the peak temperatures are only about 1850 K. As measured from

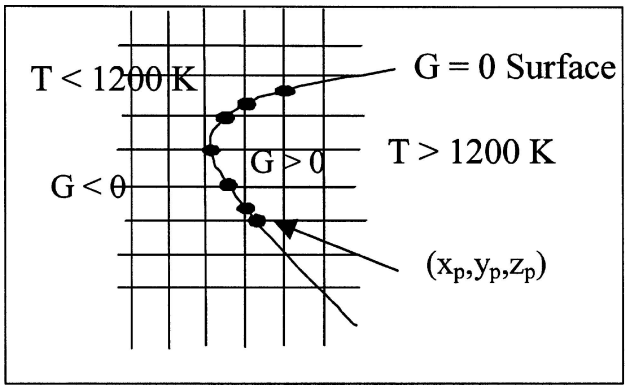

Fig. 8 Initialization of G field

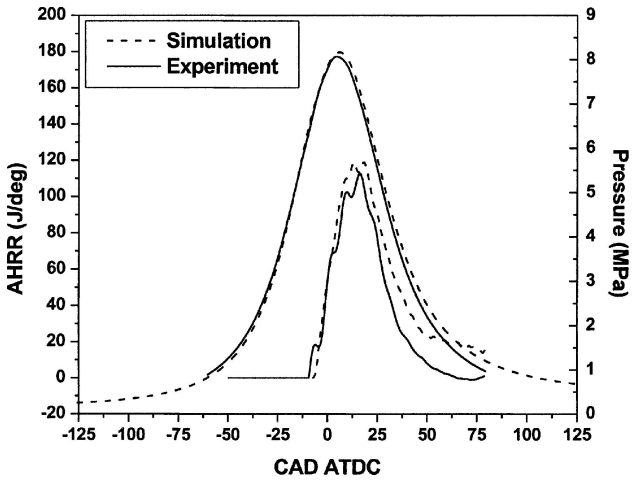

Fig. 9 Cylinder pressure and apparent heat release rate (AHRR) for case 1

Table 2 Simulated operating conditions

Case	Load (kW)	Fuel–air equivalence ratio (ϕ)	Start of injection (CA ATDC)	T_{in} (°C)	P_{in} (kPa)	Percentage diesel	Q_{pilot} (g/min)
1	21	0.47	−20	75	181	3	3.4
2	21	0.45	−20	95	181	3	3.4
3	42	0.57	−15	35	202	2	3.4
4	42	0.54	−20	35	202	2	3.4

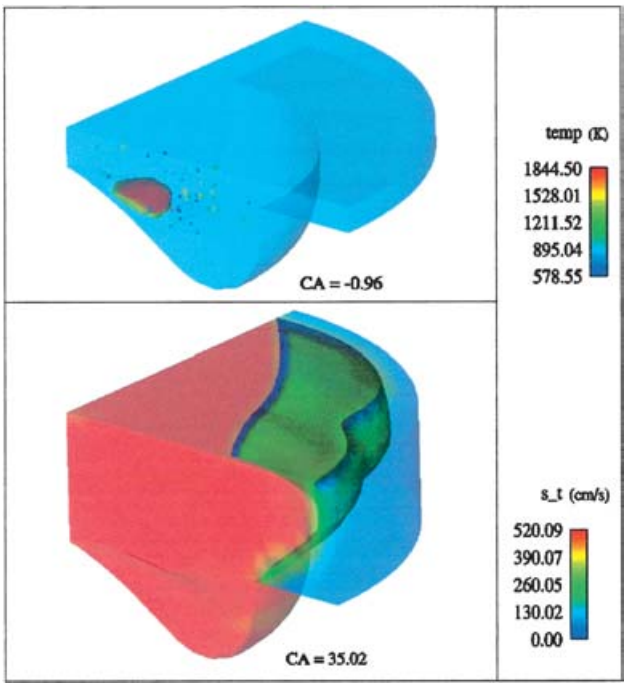

Fig. 10 In-cylinder temperature and flame structure at two different crank angles (CA). The combustion chamber surfaces are coloured with the local gas temperature (temp) and the flame surface is coloured with turbulent flame speed (s_t)

the experiments and predicted by the model, these low local temperatures result in the very low NO_x emissions given in Table 3. Predicting such low levels of NO_x emissions probably requires all the possible routes for NO_x formation and reduction. Only the extended Zel'dovich mechanism was used in this study. Considering that the extended Zel'dovich reactions account only for thermal NO_x formation, the NO_x levels predicted by the model are close to the experimental measurements. The unburned HC emissions are primarily unreacted premixed fuel, i.e. methane. The low combustion temperatures late in the expansion stroke do not favour oxidation of methane located next to the cold walls. However, the HC emissions predicted by the model are lower than their experimental levels. It should be mentioned that wall quenching and crevice flow phenomena [**28**] affect the details of late combustion and unburned HC emissions. The experimental heat release data show negligible heat release after 50° ATDC while the model still predicts finite heat release. Thus, model improvements to account for flame–wall interactions could further improve the accuracy of the model predictions in the present dual-fuel combustion simulations.

Table 3 Measured and predicted NO_x and HC emissions (exp. = experimental, sim. = simulation)

Emissions (g)	Case 1	Case 2	Case 3	Case 4
NO_x (exp.)	1.95e − 4	3.15e − 4	4.71e − 4	8.22e − 4
NO_x (sim.)	2.7e − 4	4.26e − 4	7.38e − 4	7.0e − 4
HC (exp.)	3.96e − 2	2.85e − 2	1.11e − 2	1.57e − 2
HC (sim.)	2.83e − 2	2.34e − 2	0.87e − 2	1.42e − 2

Figure 11 shows the cylinder pressure and heat release results of case 2 in which a higher intake temperature (95 °C) was set. It is very interesting to note that increased intake temperature does not result in earlier start of combustion. For both 75 and 95 °C, the combustion starts at −2° ATDC. The authors believe that when diesel fuel is injected close to TDC, the compression temperatures are high enough for both the intake temperature settings to initiate auto-ignition of diesel fuel. Therefore, the ignition delay is mainly controlled by the mixing of diesel with air. As the overall in-cylinder fluid motion is almost the same, the change in intake charge temperature from 75 to 95 °C does not have a great impact on diesel–air mixing and start of ignition. But increased intake temperature resulted in higher peak temperature of combustion as shown in Fig. 12. As expected, a substantial increase in engine-out NO_x emissions and a moderate decrease in HC were obtained in the measurements and predictions (see Table 3).

Figures 13 and 14 show the results of full load cases at different injection timings, i.e. cases 3 and 4. The overall agreement is reasonable considering that the same model constants are used for the different load and intake conditions, although the discrepancy in engine rate of heat release for case 3 leads to larger discrepancies in the NO_x emissions predictions, as seen in Table 3. The experimental results show that advancing the injection timing from −15° ATDC to

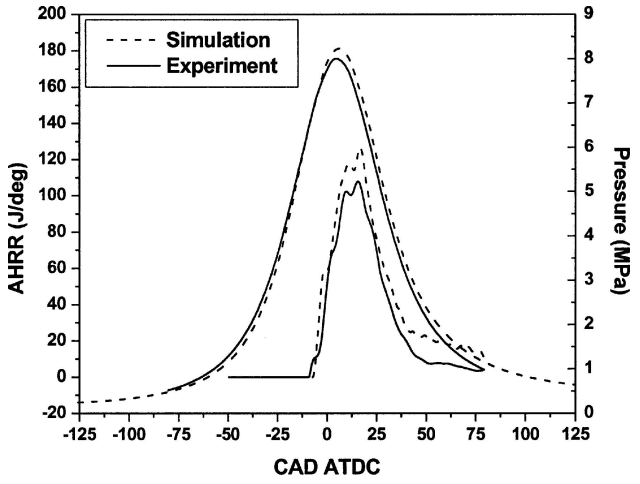

Fig. 11 Cylinder pressure and apparent heat release rate (AHRR) for case 2

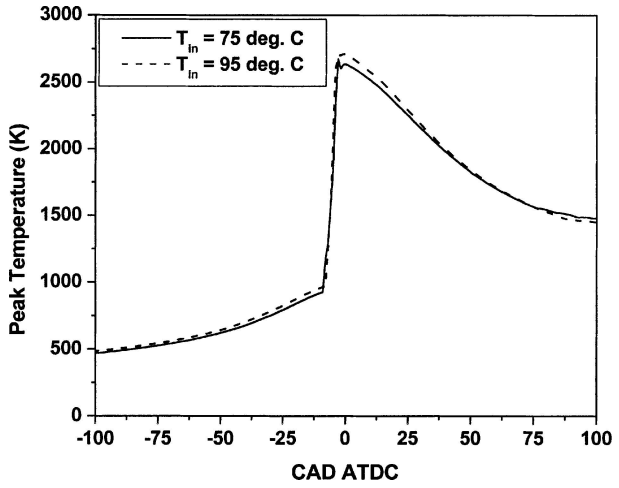

Fig. 12 Peak cylinder gas temperatures for cases 1 and 2

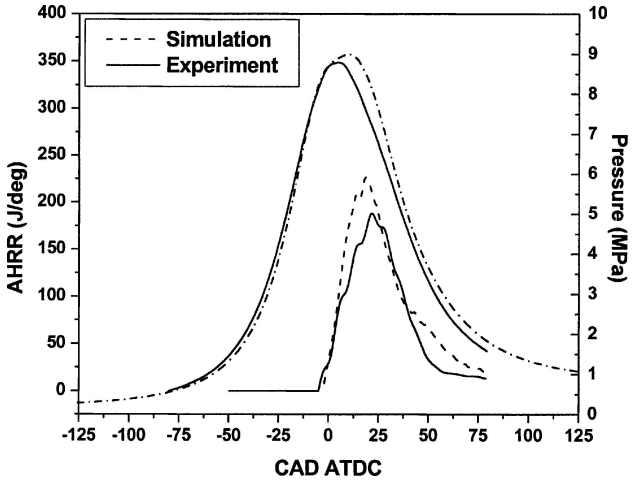

Fig. 13 Cylinder pressure and apparent heat release rate (AHRR) for case 3

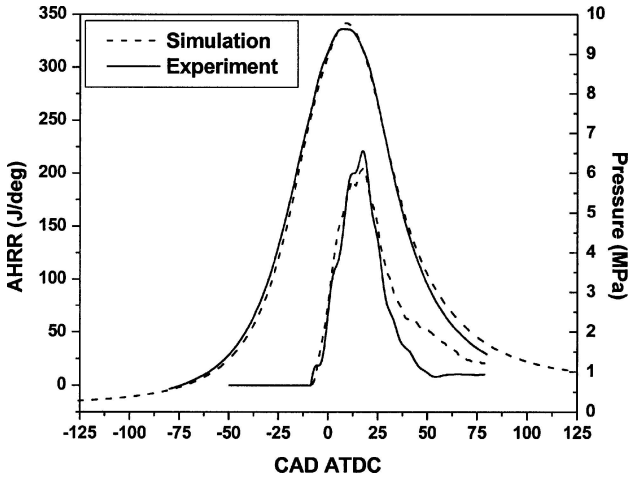

Fig. 14 Cylinder pressure and apparent heat release rate (AHRR) for case 4

-20° ATDC leads to increased NO_x emissions. But the model does not predict this trend. The model predicts almost the same amount of NO_x for both cases 3 and 4. As said previously, this is due to the fact that the model predicted heat release rates for case 3 are higher than experimental heat release rates. The higher simulated rates of heat release in Figs 9, 11, and 13 are probably due to the higher burning rates predicted by the model. Higher burning rates could be due to higher flame speeds predicted by the model than they may have actually been in the experiment or due to a different extent of fuel oxidation predicted at the flame front when compared to the experiment.

8 CONCLUSIONS

A flame propagation model based on the level set method was implemented in the KIVA-3V CFD code and applied for dual-fuel engine modelling. The model accounts for diesel spray ignition phenomena and the subsequent flame propagation in a premixed natural gas mixture. The model was found to predict combustion and emissions at low diesel pilot quantities reasonably well. The validation conditions included different engine loads, start-of-diesel-pilot-injection timings, and intake conditions. The study found that accurate laminar flame speed data are required to predict flame propagation rates and the present model could be further improved by considering the details of flame–wall interactions and crevice flow contributions that affect late combustion and unburned HC emissions.

ACKNOWLEDGEMENTS

The authors acknowledge Caterpillar Incorporated for financial support for the research. The authors would also like to thank Dr Zhichao Tan for his valuable contributions in the model development and especially S. R. Krishnan and Professor K. C. Midkiff at The University of Alabama for providing experimental data for model validation.

REFERENCES

1 **Singh, S., Kong, S. C., Reitz, R. D., Krishnan, S. R.,** and **Midkiff, K. C.** Modeling and experiments of dual-fuel engine combustion and emissions. SAE paper 2004-01-0092, 2004.

2 **Karim, G. A., Liu, Z.,** and **Jones, W.** Exhaust emissions from dual fuel engines at light loads. SAE paper 932822, 1993.
3 **Yasuhiro, D., Kou, T., Yuki, I., Shigeki, N., Ryoji, K.,** and **Takeshi, S.** Controlling combustion and exhaust emissions in a direct-injection diesel engine dual-fueled with natural gas. SAE paper 952436, 1995.
4 **Krishnan, S. R., Birudugant, M., Mo, Y., Bell, S. R.,** and **Midkiff, K. C.** Performance and heat release analysis of a pilot ignited natural gas engine. *Int. J. Engine Res.*, 2002, **3**(3), 171–184.
5 **Abd-Alla, G. H., Soliman, H. A., Badr, O. A.,** and **Abd-Rabbo, M. F.** Effect of pilot fuel quantity on the performance of a dual fuel engine. *Energy Conversion and Managmt*, 2000, **41**, 559–572.
6 **Singh, S.** *The effect of fuel injection timing and pilot quantity on the pollutant emissions from a pilot-ignited natural gas engine.* Masters Thesis, The University of Alabama, USA, 2002.
7 **Hountalas, D. T.** and **Papagiannakis, R. G.** A simulation model for the combustion process of natural gas engines with pilot diesel fuel as an ignition source. SAE paper 2001-01-1245, 2001.
8 **Hountalas, D. T.** and **Papagiannakis, R. G.** Development of a simulation model for direct injection, dual fuel, diesel-natural gas engines. SAE paper 2001-01-0286, 2001.
9 **Zhang, Y., Kong, S. C.,** and **Reitz, R. D.** Modeling and simulation of a dual-fuel (diesel/natural gas) engine with multidimensional CFD. SAE paper 2003-01-0755, 2003.
10 **Fraser, R. A., Siebers, D. L.,** and **Edwards, C. F.** Auto-ignition of methane and natural gas in a simulated diesel environment. SAE paper 9102271, 1991.
11 **Naber, J. D., Siebers, D. L., Caton, J. A., Westbrook, C. K.,** and **Di Julio, S. S.** Natural gas auto-ignition under diesel condition: experiments and chemical kinetic modeling. SAE paper 942034, 1994.
12 **Westbrook, C. K.** and **Dryer, F. L.** Prediction of laminar flame properties of methane–air mixtures. *Combst. Flame*, 1980, **37**(171), 171–192.
13 **Zhou, G.** and **Karim, G. A.** A comprehensive kinetic model for the oxidation of methane. In Proceedings of the Energy Sources Technology Conference, *Emerging Energy Technology*, 23–26 January 1994, New Orleans, Louisiana, Vol. 57 (American Society of Mechanical Engineers, New York).
14 **Peters, N.** and **Rogg, R. (Eds)** *Reduced reactions mechanisms for applications in combustion systems, lecture notes in physics*, Vol. 15, 1993 (Springer-Verlag).
15 **Micklow, G. J.** and **Gong, W.** Mechanism of hydrocarbon reduction using multiple injection in a natural gas fuelled/micro-pilot diesel ignition engine. *Int. J. Engine Res.*, 2002, **3**(1), 13–21.
16 **Peters, N.** *Turbulent combustion*, 2000 (Cambridge University Press, UK).
17 **Tan, Z.** and **Reitz, R. D.** Modeling ignition and combustion in spark-ignition engines using a level set method. SAE paper 2003-01-0722, 2003.
18 **Kong, S. C.** and **Reitz, R. D.** Multidimensional modeling of diesel ignition and combustion using a multistep kinetics model. *J. Engng Gas Turbines and Power*, 1993, **115**, 781–789.
19 **Patterson, M. A.** and **Reitz, R. D.** Modeling the effects of fuel spray characteristics on diesel engine combustion and emissions. SAE paper 980131, 1998.
20 **Han, Z. Y.** and **Reitz, R. D.** A temperature wall function formulation for variable-density turbulent flows with application to engine convective heat transfer modeling. *Int. J. Heat and Mass Transfer*, 1997, **40**(3), 613–625.
21 **Amsden, A.** KIVA-3V: A block structured KIVA program for engine with vertical or canted valves, report LA-13313-MS, Los Alamos National Laboratories, USA, 1997.
22 **Kong, S. C., Han, Z. W.,** and **Reitz, R. D.** The development and application of a diesel ignition and combustion model for multidimensional engine simulations. SAE paper 950278, 1995.
23 **Halstead, M., Kirsh, L.,** and **Quinn, C.** The auto-ignition of hydrocarbon fuels at high temperatures and pressures: fitting of a mathematical model. *Combust. Flame*, 1977, **30**, 45–60.
24 **Tan, Z.** and **Reitz, R. D.** Development of a universal turbulent combustion model for premixed and direct injection spark/compression ignition engines. SAE paper 2004-01-0102, 2004.
25 **Rahim, F., Elia, M., Ulinski, M.,** and **Metghalchi, M.** Burning velocity measurements of methane–oxygen–argon mixtures and an application to extend methane–air burning velocity measurements. *Int. J. Engine Res.*, 2002, **3**(2), 81–92.
26 **Kee, R. J., Gracer, J. F., Miller, J. A., Meeks, E.,** and **Smooke, M. D.** *PREMIX: A Fortran code for modeling steady one-dimensional premixed flames*, 1998 (Reaction Design, California, USA).
27 **Heywood, J. B.** *Internal combustion engine fundamentals*, 1988 (McGraw Hill, New York).
28 **Reitz, R. D.** and **Kuo, T.-W.** Modeling of HC emissions due to crevice flows in premixed-charge engines. SAE paper 892085, 1989.

APPENDIX

Notation

A	area of flame in cell
AHRR	apparent heat release rate
ATDC	after top dead centre
c_p	heat capacity
CAD	crank angle degree
D_t	turbulent diffusivity
Da	DamKohler number

f	combustion progress variable
I	integral length scale
I_F	laminar flame thickness
j	computational cell or vertex index
$\tilde{k}_M$	curvature of the mean flame front
Q_{pilot}	diesel pilot quantity
R	radius of ignition kernel
s_t^0	turbulent flame speed
T_u	unburned gas temperature
V	volume of cell
$\boldsymbol{v}_{vertex}$	velocity of moving cell vertex
$\boldsymbol{v}_{bf}$	bulk flow velocity
x_p, y_p, z_p	x, y, and z coordinates of $G = 0$ location
Y_i^u	concentration of species i in unburned mixture
Y_i^b	concentration of species i in burned mixture
Y_i^*	local and instantaneous thermodynamic equilibrium concentration of species i
λ	heat conductivity
ρ	density
τ_l	laminar kinetic timescale
τ_t	turbulent timescale, $C_{m2}k/\varepsilon$
ϕ	fuel–air equivalence ratio

Subscripts and superscripts

b	burned
bf	bulk flow
i	species index
l	laminar
M	mean
t	turbulent
u	unburned